THE JOURNAL OF PHYSICAL CHEMISTRY C

Article

pubs.acs.org/JPCC

Fe K-Edge X-ray Absorption Spectroscopy Study of Nanosized Nominal Magnetite

C. Piquer,[†] M. A. Laguna-Marco,[†] A. G. Roca,[‡,§] R. Boada,[†,∥] C. Guglieri,[†] and J. Chaboy*[,†,⊥]

[†]Instituto de Ciencia de Materiales de Aragón, Consejo Superior de Investigaciones Científicas - Universidad de Zaragoza, 50009 Zaragoza, Spain

[‡]Centro de Investigaciones Biomédicas en Red (CIBER BBN), Campus Río Ebro, 50018, Zaragoza, Spain

[⊥]Departamento de Física de la Materia Condensada, Un. Zaragoza, 50009 Zaragoza, Spain

Supporting Information

ABSTRACT: When studying nominal magnetite nanoparticles, it is mandatory to obtain a precise structural characterization to get an accurate relationship with their physiochemical properties. The great deal of information accumulated to date on the characterization of nominal magnetite and maghemite NPs does not clarify if the synthesized materials are single o multiphase systems involving bulk-like stoichiometric oxides (Fe_3O_4, γ-Fe_2O_3, α-Fe_2O_3, ...), or single or multiphase entities formed by nonstoichiometric oxides. In this work we propose a new approach to determine the structure of Fe oxide NPs by using the Fe K-edge X-ray absorption near edge spectroscopy. We report here an X-ray absorption near edge spectroscopy study at the Fe K- and $L_{2,3}$-edges, on nominal magnetite nanoparticles synthesized by different methods. In addition, X-ray magnetic circular dichroism was recorded at the Fe $L_{2,3}$-edges, in selected samples. We have found that the experimental spectra are not well reproduced by any linear combination of the absorption spectra of Fe_3O_4 and γ-Fe_2O_3 bulk references, even taking into account other oxides as goethite or ferrihydrite. The analysis of the Fe K-edge XANES spectra shows that it is the size, and not the synthesis method, which determines the structure of the NPs. Our experimental results indicate that, irrespective of the synthesis method, the nominal magnetite NPs are, actually, a single phase non stoichiometric $Fe_{3-\delta}O_4$ oxide. At the origin of this phase are the cation vacancies, which lead to the modification of the structural arrangements at the Fe sites with respect to those found in bulk-like iron oxides.

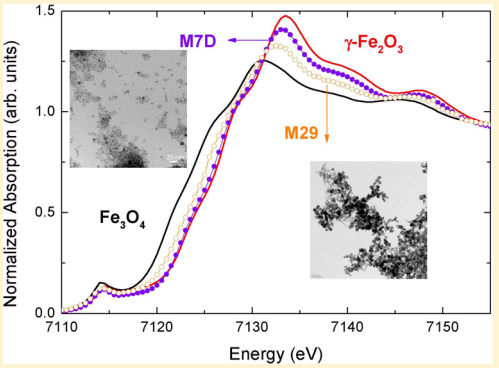

INTRODUCTION

Magnetic nanoparticles (NPs) are nowadays the subject of extensive research because of their promising applications in many technological areas.[1] The possibility of using NPs as nanodiagnostic or nanotherapeutic tools centers a great interest in the biomedical field.[2] In particular, iron oxide, in the form of magnetite (Fe_3O_4) and maghemite (γ-Fe_2O_3), has been revealed as an ideal material because of its biocompatibility and easy removal from the body after its use following natural routes.[3]

The structural and physicochemical properties of the nanoparticles determine to a great extent their biofunctionality, being these properties associated with the average particle size, size distribution, shape, crystal order, surface properties, and the presence of bonded molecules at the surface. Similarly, the dependence of the magnetic properties of iron oxide nanoparticles on different parameters as the degree of structural order at the surface and inside the particles has been also reported.[4] However, despite the fact that these parameters can be controlled, in principle, with the synthesis method,[4,5] the current description of these relationships is still rather vague. In this way, obtaining a precise characterization of these structural details in monodisperse nanocrystals, as a previous step to get an accurate relationship with their magnetic properties, is nowadays one of the most challenging open issues in the field.

This is of particular relevance in the case of monodisperse iron oxide nanocrystals. The great deal of information accumulated to date on the characterization of magnetite and maghemite NPs does not clarify if the synthesized materials are single or multiphase systems involving bulk-like oxides (Fe_3O_4, γ-Fe_2O_3, α-Fe_2O_3, ...) or multiphase entities formed by nonstoichiometric oxides.[6−9] Very often the characterization of iron oxide magnetic nanoparticles is made by combining infrared (IR) and Mössbauer spectroscopies with X-ray diffraction (XRD) and transmission electron microscopy (TEM).[10,11] However, the standard methods that we have for solving the atomic structure of bulk crystals fail for such materials due to nanoscale effects arising from the inherently very small crystallite sizes, the large surface-to-volume ratio, near-surface relaxation, local lattice distortions, and so on, and broadening and smearing out the Bragg reflections in the XRD patterns or the Mössbauer lines.[12] This renders critical in the

Received: October 23, 2013
Revised: December 16, 2013
Published: December 19, 2013

dx.doi.org/10.1021/jp4104992 | J. Phys. Chem. C 2014, 118, 1332−1346

case of magnetite and maghemite nanoparticles as they may show structural disorder that can substantially modify the properties of the materials, and consequently, they cannot be simply considered as small pieces of bulk material. In addition to this, the existence of several polymorphs and their possible transformation through oxidation makes this problem further complicated. While the conversion of magnetite to maghemite on micrometer- or close-to-micrometer-sized particles has been well characterized, the same does not hold for ultrafine magnetite powders for which several Mössbauer experiments indicate the occurrence of partial oxidation, including the formation of nonstoichiometric phases.[7−9,13,14] Similarly, controversial results regarding the capability to distinguish Fe_3O_4 from γ-Fe_2O_3 have been also reported when both IR or Raman spectroscopies have been used to characterize the samples.[15−19] Finally, it is worth mentioning that no general consensus exists regarding the oxidation mechanism of magnetite. The magnetite to hematite transformation has been proposed either to proceed directly or through the conversion of magnetite to maghemite and the subsequent conversion to hematite.[18,20−23] Moreover, it has been also reported that magnetite seems to oxidize to maghemite via short-live "hydroxo" intermediate.[24]

These uncertainties make clear that more powerful experimental tools are needed to obtain an accurate structural and magnetic characterization of these iron oxide NPs. These tools include X-ray absorption near-edge spectroscopy (XANES), extended X-ray absorption fine structure (EXAFS), and magnetic X-ray circular dichroism (XMCD). Early studies by van Aken et al. proposed different methods to obtain the quantification of ferrous/ferric ratios in minerals at submicrometre scale by analyzing the intensity ratio of the Fe $L_{2,3}$-edge XAS spectra.[25,26] In principle, the $L_{2,3}$-edges XAS spectral shape may provide information about the oxidation state and the symmetry of the Fe transition metal ions, and XMCD at these absorption edges allows to separate the contributions of the magnetic moments of Fe ions in tetrahedral and octahedral sites.[25,27,28] However, for the most common iron oxides (γ-Fe_2O_3, Fe_3O_4, α-Fe_2O_3, FeO(OH), ...) the $L_{2,3}$-edges XAS spectra are very similar. Therefore, upon the coexistence of several iron oxide phases in the same material, the possibility of extracting accurate quantitative information about the structural composition of the material gets complicated. Likewise, the $L_{2,3}$-edge XMCD for γ-Fe_2O_3 and Fe_3O_4 are very similar and, therefore, the possibility of making a fine analysis is seriously concerned when several phases are present in the sample. Besides, the presence of antiferromagnetic oxides, as α-Fe_2O_3 or FeO(OH), may also affect the normalization of the XMCD signals. Indeed, the analysis of the XMCD spectra of magnetite Fe_3O_4 centers a hot debate that extends to the dissimilarity of the reported experimental spectra.[29−34] Recent XMCD studies performed at the Fe $L_{2,3}$-edges on 5 nm magnetite nanoparticles synthesized by different methods suggested the presence of up to 50% of maghemite.[35] This is in contrast with the 20% estimates obtained from Mössbauer spectroscopy on the same samples.[36] Beyond this quantitative disagreement, these works suggest the simultaneous presence of both magnetite and maghemite in the samples. Accordingly, the possibility of obtaining pure stoichiometric magnetite for particle sizes below a few tens of nanometers is seriously concerned, in agreement with the early work of Park et al.[29] These authors suggested that magnetite and maghemite form a mixture in the form $(\gamma\text{-}Fe_2O_3)_{1-x}(Fe_3O_4)_x$, in such a way that maghemite is the dominant phase of the small 5-nm iron oxide nanocrystals, whereas the proportion of the magnetite component gradually increases as the particle size does. Unfortunately, these experiments did not determine if this mixture corresponds to a multiphase Fe_3O_4 + γ-Fe_2O_3 system in which each component retains its bulk properties or, on the contrary, we stand in front of a nonstoichiometric phase whose magnetic properties cannot be simply derived from the values of bulk Fe_3O_4 and γ-Fe_2O_3.

This uncertainty in the phase determination prevents establishing a definitive correlation between the magnetic properties and the nanostructure details of the iron oxide NPs. Very often it is assumed, making a parallel to the case of metal/oxidized iron NPs,[37] that the structure of iron oxide nanoparticles consists in a core of magnetite, while the surface is partially oxidized. This leads to the proposition of different core−shell models ranging from a simply bulk-like magnetite−maghemite core−shell structure.[6,38] to others, including a magnetic core and a nonmagnetic shell, where the magnetic dead layer should account for the observed decrease of the magnetization of the nanoparticles as compared to the bulk materials.[39] However, the variation of the shell thickness with the particle size is controversial,[40,41] as it is the fact that for decreasing particle size below 50 nm the Verwey transition is no longer observable.[42] Consequently, it renders clear the need of obtaining a precise determination of the nanostructure details of the iron oxide NPs prior to accounting for their magnetic properties. Hence, we propose in this work a different approach to determine the structure of Fe oxide NPs. We have performed a XANES study at the Fe K-edge in several magnetite/maghemite NPs synthesized by different methods. Our main objective is to determine if the nominal Fe_3O_4 nanoparticles are single or multiphase systems and the nature of these phases. More specifically, if the different components can be regarded as well-defined, stoichiometric, bulk-like oxides or, on the contrary, they consist of nonstoichiometric oxides.

Fe K-edge X-ray absorption spectroscopy (XAS) has been widely used for the analysis of iron speciation in complex natural mixtures such as soils and sediments.[43−45] In contrast, few studies have exploited the powerful characteristics of the XAS at the Fe K-edge for determining components and their relative proportions in magnetite and maghemite nanoparticles.[46,47] The main advantage of using Fe K-edge absorption instead of that at the $L_{2,3}$-edges for such a structural determination is 2-fold. First, the Fe K-edge spectral shape is more sensitive to the geometrical details of the absorbing site (overall symmetry, distances and bond angles) than the Fe $L_{2,3}$-edge absorption, which is mainly governed by the point symmetry at the absorbing site (octahedral and tetrahedral in this case). In addition, for a similar coordination, there is a chemical shift of about ∼3−4 eV between Fe^{3+} and Fe^{2+} XANES spectra, which is easily experimentally detected.[48−51] Second, the probing depth at the $L_{2,3}$ edges of iron is typically of ∼45 Å in the case of iron oxides.[52] Consequently, contribution from the atoms at the surface is emphasized in the absorption and dichroism signals at these edges. The K-edge spectra, on the other hand, probe the whole nanoparticle.[46] Therefore, by tuning the XAS absorption at the Fe K-edge it should be also possible to monitor how the relative amount of the different oxide phases, if present, varies with both the preparation method and the size of the particles.

dx.doi.org/10.1021/jp4104992 | J. Phys. Chem. C 2014, 118, 1332−1346

EXPERIMENTAL SECTION

The iron oxide nanoparticles were obtained using different wet synthesis methods of common use in nanotechnology, namely, precipitation, coprecipitation, and thermal decomposition. It is worth noticing that the wet chemical procedures for synthesizing iron oxide nanoparticles allow a significant control over size and composition of the final product that grants their use in different applications.[53] Likewise, Roca et al.[54] have reported that thermal decomposition and coprecipitation methods produce nanoparticles within the same size range (3−18 nm), being spherical, isolated, and nearly monodisperse in the case of thermal decomposition.

Samples obtained using the precipitation technique were synthesized diluting a mass of iron(II) sulfate heptahydrate ($FeSO_4{\cdot}7H_2O$, >99%, Sigma-Aldrich) in milli-Q water (Millipore) at pH 7 using NaOH and potassium nitrate (KNO_3, Sigma-Aldrich) as mild oxidant.[55] With this method, iron oxide magnetic nanoparticles with mean crystallite size D_{XRD} of 29 and 31 nm were synthesized. These samples were termed M29 and M31, respectively.

The coprecipitation process involves the joint hydrolysis of iron(II) and iron(III) salts in alkaline conditions. For synthesis, 4.4 g of iron(III) chloride hexahydrate ($FeCl_3{\cdot}6H_2O$, >98%, Sigma-Aldrich) and iron(II) chloride tetrahydrate ($FeCl_2{\cdot}4H_2O$, >98%, Sigma-Aldrich) were placed in 61 mL of milli-Q water, which was previously deareated using Ar gas flow. The obtained solution was further purged with Ar gas to prevent oxidation of Fe^{2+} ions. After purging for 60 min, a volume of a 2 M NaOH solution was added dropwise up to pH 9 and the change in suspension's color was observed to dark brown and further black.[56−58] The black iron oxide product responded to magnetic fields as expected. Nanoparticle sizes were tuned after adjustments in the concentration of alkali and mixed iron salts for synthesizing iron oxide magnetic nanoparticles with mean D_{XRD} between 4 and 7 nm. These samples were labeled M4, M6, and M7.

The thermal decomposition procedure has been applied for the synthesis of spherical nanoparticles and briefly consists in the use of metal−organic and organometallic iron precusors in organic environments and in the presence of surfantants. Iron oxide nanoparticles of 7, 9, 12, and 18 nm in meansize (labeled M7D, M9D, M12D, and M18D, respectively) were synthesized by thermal decomposition of iron organic compounds in organic solvents in the presence of surfactants. Different solvents were chosen for tuning the particle size.[59] Finally, magnetite transformation to maghemite was triggered after synthesis using a thermal treatment in air at 150 °C for 24 h. Materials termed G7D, G29, and G31 were obtained from the thermal oxidation of M7D, M29, and M31, respectively.

Magnetic nanoparticles and nanocomposites were imaged in a 200 keV FEI Tecnai T20 transmission electronic microscope to study their size, polydispersity, and shape. To prepare the samples for this technique, one drop of a dilute suspension of nanoparticles dispersed in ethanol was placed on a carbon-coated copper grid and allowing the solvent to evaporate slowly at room temperature. Mean particle size was calculated from TEM data obtained by measuring the largest internal dimension of at least 150 particles. X-ray patterns were collected at room temperature between 10° and 80° in a Rigaku D-Max system. The X-ray system was working at 40 kV and 100 mA with a counting rate of 4 s $step^{-1}$, and Cu Kα radiation was selected by using a graphite monochromator (λ = 1.5406 Å). To prepare the samples, an aliquot of the suspension was dried at room temperature until solvent was evaporated. XRD provides information about the iron oxide phase of the nanoparticles and its crystal size (D_{XRD}). D_{XRD} was calculated from the broadening of the (311) reflection of the spinel structure following standard procedures.

Fe K-edge XAS experiments were performed at the beamline BL39XU of the SPring-8 Facility. XANES spectra were recorded at room temperature in the transmission mode and by using a Si(220) monochromator. The energy of the absorption spectra was calibrated by measuring the XANES of a Fe metal foil. For the measurements, homogeneous layers of the powdered samples were made by spreading fine powders of the material onto an adhesive tape. Thickness and homogeneity of the samples were optimized to obtain the best signal-to-noise ratio. XANES spectra were recorded on the nanoparticles and on a series of bulk iron oxide references: Fe_3O_4 (magnetite), α-Fe_2O_3 (hematite), γ-Fe_2O_3 (maghemite), FeO(OH) (goethite), ferrihydrite, FeO (wüstite), and $FeCO_3$ (siderite). The absorption spectra were analyzed according to standard procedures[60] by using the ATHENA program package.[61] It should be noted that these measurements are in perfect agreement with previous test measurements performed at the BM25A SpLine beamline of the ESRF. No modification of the XAS spectra, other than the signal-to-noise ratio and energy resolution, has been found on the same specimens measured at the initial run and up to three years later, neither in different specimens prepared from the same sample. This indicates that the observed properties are intrinsic and stable in time, that is, no time-dependent oxidation has been observed. It should be also noted that our XANES measurements performed on the bulk reference oxides perfectly agree with those previously reported.[37,43,44] In addition, Fe $L_{2,3}$-edge XAS and XMCD measurements on samples M9D and M18D were performed at the beamline 4ID-C of the Advanced Photon Source at Argonne National Laboratory. XMCD spectra were recorded in the TEY mode at T = 7 K and under the action of an applied magnetic field (H = ±1 T and ±3 T). For the measurements, samples were prepared as pellets of homogeneous fine powders of the materials slightly diluted in BN (boron nitride). The pellets were mounted on the sample holder by using carbon tape.

The computation of the Fe K-edge XANES spectra was carried out using the multiple-scattering program CONTINUUM[62] included in the MXAN program package.[63] A complete discussion of the procedure can be found elsewhere.[64−66] The potential for the different atomic clusters was approximated by a set of spherically averaged muffin-tin (MT) potentials built by following the standard Mattheis' prescription. The muffin-tin radii were determined following the Norman's criterion. During the computations special attention has been paid to determine the best choice for the overlapping factor between the muffin-tin spheres and for the exchange and correlation part of the final state potential.[67−70] We have found that the best agreement between the computations and the experimental spectra is obtained by using an overlapping factor of 1% and the Dirac-Hara ECP potential, in agreement to previous works for transition metal oxides and related compounds.[69,71−74] It should be stressed that no free parameter has been used during the calculations. The theoretically calculated spectra have been directly compared to the experimental XANES spectrum, that is, no fitting procedure has been used. The assessment of the quality of the theoretical computations is

dx.doi.org/10.1021/jp4104992 | J. Phys. Chem. C 2014, 118, 1332−1346

based on the correct reproduction of the shape and energy position of the different spectral features and of their relative energy separation and the intensity ratio. In all the cases, the theoretical spectra have been convoluted with a Lorentzian shape function to account for the core-hole lifetime (Γ = 1.25 eV)[75] and the experimental resolution (0.4 eV).

RESULTS AND DISCUSSION

The crystallite size (D_{XRD}) and physical particle size (D_{TEM}) of the synthesized iron oxide nanoparticles were determined by XRD and TEM, respectively. The crystallite sizes calculated from the Scherrer's equation are summarized in Table 1. Representative X-ray diffractograms and TEM images can be found in the Supporting Information.

Table 1. Crystallite Size (D_{XRD}) and Physical Particle Size (D_{TEM}) of the Synthesized Nanoparticles Determined by XRD and TEM, Respectively[a]

method	sample	D_{XRD} (nm)	D_{TEM} (nm)	w (±0.02)
coprecipitation	M4	4.3 ± 0.2	4.8	0.17
	M6	6.8 ± 0.3	6.6	0.26
	M7	7.1 ± 0.3	5.8	0.23
precipitation	M29	29 ± 2	33	0.21
in aq. media	M31	31 ± 2	42	0.27
thermal	M7D	7.2 ± 0.5	6.8	0.14
decomposition	M9D	9.4 ± 0.4		
	M12D	11.5 ± 0.5		
	M18D	18 ± 1	18	0.21
oxidation	G7D	7.8 ± 0.2		
treatment	G29	29 ± 2		
	G31	31 ± 2		

[a] w, the standard deviation of log D_{TEM}, is an indicator of the degree of polydispersity.

Fe $L_{2,3}$-Edge XAS and XMCD Characterization. The Fe $L_{2,3}$-edges XAS and XMCD spectra recorded on the nanoparticles are reported in Figure 1. For the sake of comparison the XAS and XMCD spectra of reference bulk samples are also displayed.[76,77] The Fe $L_{2,3}$-edge XAS and XMCD spectra of our samples are similar to those previously reported in similar systems.[29,35] The XMCD spectra show the characteristic spectral profile of both magnetite and maghemite, that is, the occurrence of three main peaks with negative (n_1), positive (p_2), and negative (n_3) intensity as energy increases. These peaks and their relative intensities are typically accounted for in terms of the site occupancies of the Fe cations in the spinel structure (Fe^{2+}-O_h, Fe^{3+}-T_d, and Fe^{3+}-O_h).[27,31,78−82]

Starting from the fair agreement between multiplet calculations and experimental XMCD on bulk iron oxides,[27,28] the XMCD of iron oxides NPs are often modeled by a linear combination of the three aforesaid Fe contributions. Following this method Park et al. characterized monodisperse iron oxide nanocrystals as a mixture of magnetite and maghemite in the form $(\gamma\text{-}Fe_2O_3)_{1-x}(Fe_3O_4)_x$ whose relative amounts vary as a function of the NPs size.[29] In our case, the most significant difference in the XMCD of both M9D and M18D compounds and those of magnetite and maghemite lies in the relative intensity of the negative n_1 and n_3 peaks: the n_1/n_3 intensity ratio is ∼0.8, while it is ∼0.4 and 1.5 for maghemite and magnetite, respectively. If one considers that these oxide nanocrystals corresponds to the proposed $(\gamma\text{-}Fe_2O_3)_{1-x}(Fe_3O_4)_x$ mixture,[29] we find a significant amount of maghemite in the samples, ∼ 70%, in agreement with previous findings.[35] However, although the n_1/n_3 ratio coincides for both M9D and M18D samples the overall amplitude of the XMCD signals of the M18D is decreased by an ∼1.2 factor with respect to that of the M9D sample. The picture emerging from the comparison of the overall intensity of the XMCD data is that the iron magnetic moment in sample M18D significantly

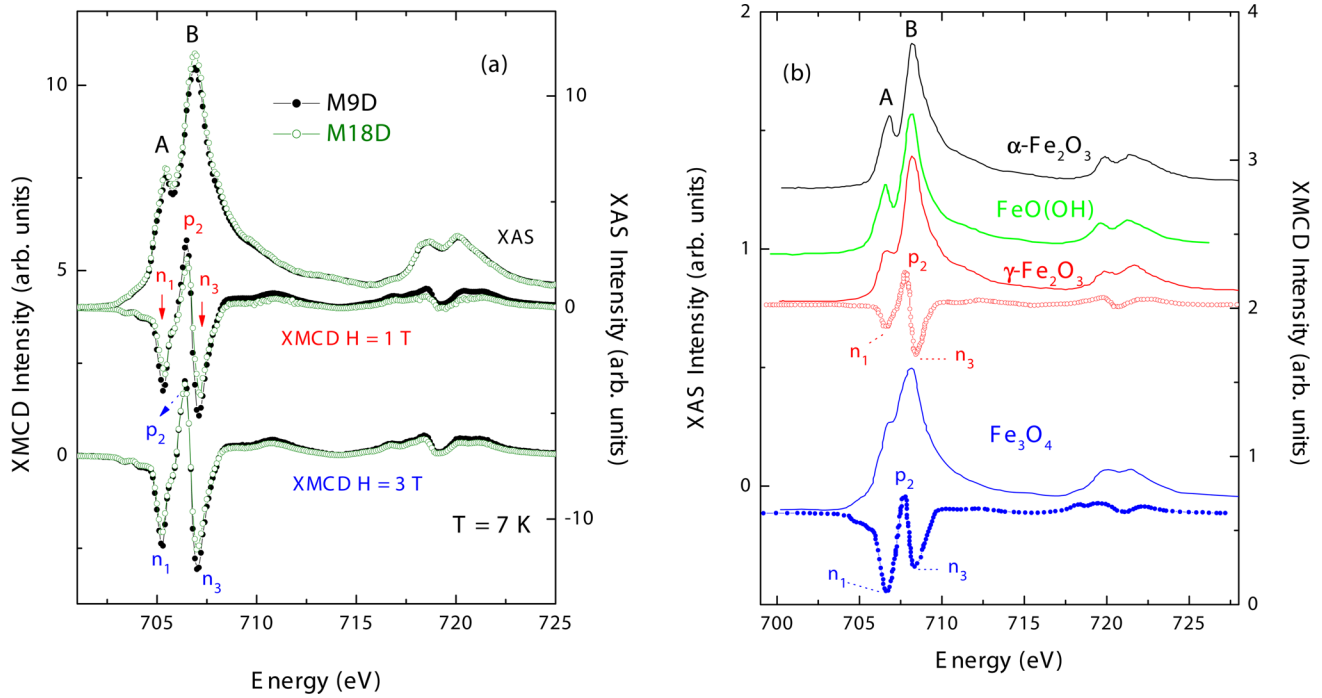

Figure 1. (a) Comparison of the Fe $L_{2,3}$-edges XAS and XMCD spectra recorded for M9D and M18D samples. (b) Comparison of the Fe $L_{2,3}$-edges XAS and XMCD spectra of reference bulk samples (adapted from Kim et al.[76] and Chang et al.,[77] respectively).

dx.doi.org/10.1021/jp4104992 | J. Phys. Chem. C 2014, 118, 1332−1346

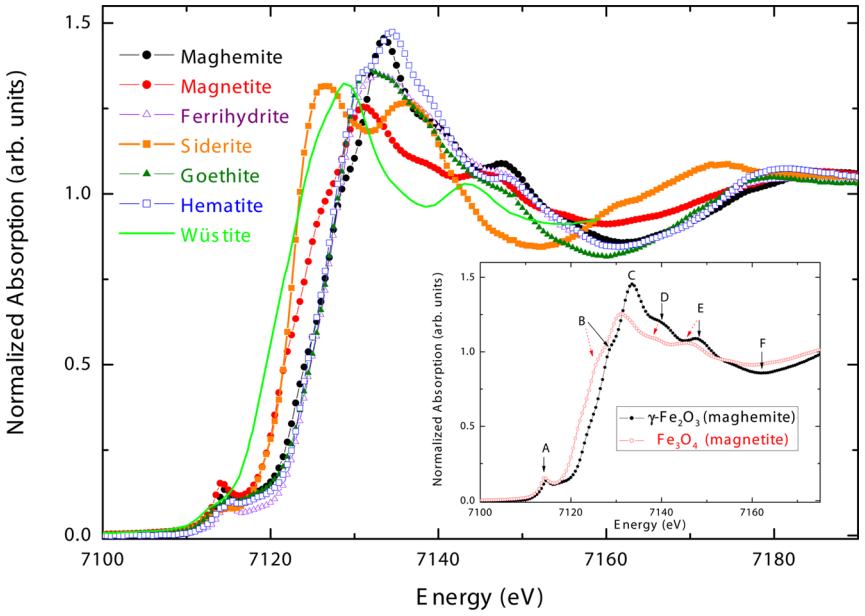

Figure 2. Comparison of the experimental Fe K-edge XANES spectra of several iron oxide bulk references. In the inset, a detailed comparison of the experimental Fe K-edge XANES spectra of magnetite (Fe_3O_4) and maghemite (γ-Fe_2O_3) bulk references is shown.

decreases as compared with that of the M9D one, which is difficult to reconcile with the existence of the same mixture of bulk-like magnetite and maghemite for the two compounds (same n_1/n_3 ratio). If we take into account that the intensity of the white line of the M18D XAS spectrum (after normalization to the absorption edge jump) is ∼20% higher than that obtained in the M9D, then the difference between the iron magnetic moment that one obtains by applying sum rules for M9D and M18D is even larger.[83,84] In addition, if the increase in this white line intensity is simply addressed to the enhancement of the number of 3d holes in the Fe 3d band, the existence of the same mixture of bulk-like magnetite and maghemite for the two compounds is not a consistent conclusion.

We would like to point out in this respect an experimental result that has attracted, to our knowledge, little attention in the past. As previously discussed, the XMCD spectra of nominal magnetite/maghemite NPs can be reasonably reproduced by a linear addition of the XMCD spectra of bulk magnetite and maghemite. However, the same does not hold for the XAS spectra. The XAS spectra of nominal magnetite and maghemite NPs show a sharp peak (A) in the absorption spectra that is not present in the spectra on the bulk references.[29,35,46,76,77] As a consequence, contrary to the XMCD, the XAS spectra of nominal magnetite/maghemite NPs can not be reproduced by a linear addition of the XAS spectra of bulk magnetite and maghemite. Indeed, this spectral profile with a marked A peak resembles that found in the case of antiferromagnetic α-Fe_2O_3, FeO(OH), or ferrihydrite oxides rather than those of magnetite or maghemite.[46,85,86] Therefore, while the experimental Fe $L_{2,3}$-edge XMCD spectra are compatible with the proposed $(\gamma\text{-}Fe_2O_3)_{1-x}(Fe_3O_4)_x$ scheme,[29] the same does not hold for the XAS spectra. In principle, the apparent contradiction between XMCD and XAS data might be reconciled by considering the presence of antiferromagnetic oxides in the materials that should modify the XAS line shape but not the XMCD one. If this was the case, the quantitative analysis of the XMCD spectra should be seriously concerned as the normalization of the signal and, consequently, the estimate of the Fe magnetic moment derived by applying the sum rules[83,84] would be modified. However, attempts of reproducing the experimental XAS spectra (especially regarding the intensity of peak A) as a linear combination of bulk-like reference ones, as made for the XMCD spectra, yields that the relative amount of the AFM oxides should be large enough to be detected by macroscopic tools, contrary to the experimental observations.

All in all these results show that as far as the Fe $L_{2,3}$-edge absorption is dictated by the valence and point symmetry of the absorbing sites the overall line shape of all these iron oxides are similar, which makes complicated to identify, beyond the Fe^{2+}/Fe^{3+} ratio,[25,26] the relative amount of the oxide phases present in the material. Consequently, the Fe $L_{2,3}$-edge absorption alone is not able to provide an accurate structural determination in these cases in which a mixture of non-stoichiometric and stoichiometric iron oxides might be present. Alternatively, another way of describing the observed experimental trend is to consider the partial oxidation of magnetite, in the form $Fe_{3-\delta}O_4$, allowing the appearance of vacancies in the spinel octahedral sites.[78,87,88] The oxidation of magnetite means a decrease of Fe^{2+} in octahedral sites, that is compensated by a slight increase in the occupancy of the octahedral sites by Fe^{3+}. The concomitant modification of the crystal field parameters may result in the shift of the energies of the absorption peaks[27,77,89] and, consequently, structural determinations based in the weighted addition of end-members spectra could be affected.

Fe K-Edge XANES Characterization. The higher sensitivity to the oxidation state and structural details of the Fe K-edge is illustrated in Figure 2 where the XANES spectra of several iron oxide bulk references are shown. Contrary to the Fe $L_{2,3}$-edge case, the Fe K-edge spectral shape is clearly different for all the references considered.

In particular, magnetite and maghemite show quite different XANES spectra, not only regarding the overall spectral shape but also concerning the edge position (see inset in Figure 2). The energy shift of the absorption threshold is due to the

dx.doi.org/10.1021/jp4104992 | J. Phys. Chem. C 2014, 118, 1332−1346

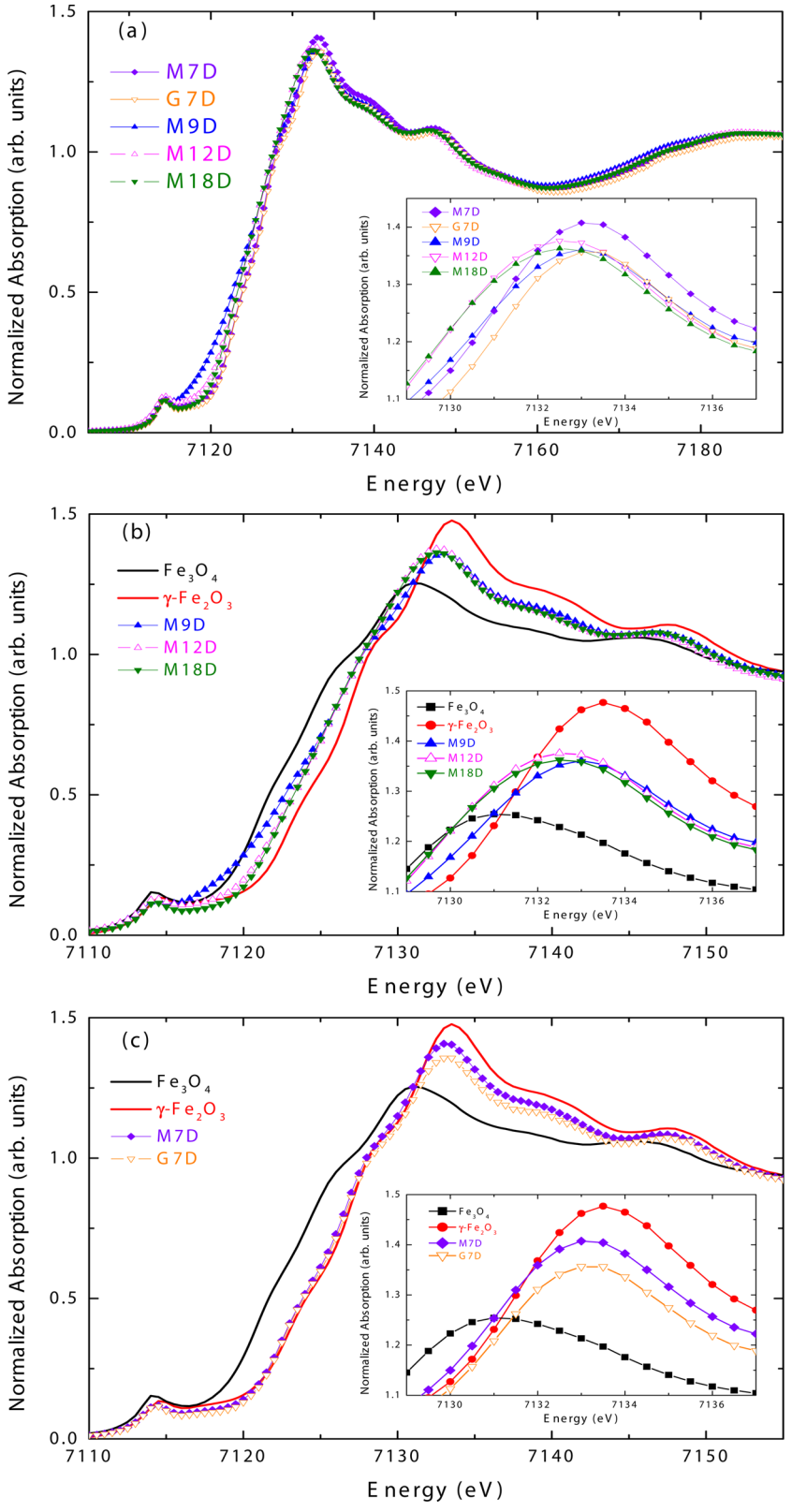

Figure 3. (a) Comparison of the experimental Fe K-edge XANES spectra of nanoparticles synthesized by thermal decomposition (M7D, M9D, M12D, and M18D) and sample G7D. (b) Detailed comparison of the experimental Fe K-edge XANES spectra of samples M9D, M12D, and M18D with those of Fe_3O_4 and γ-Fe_2O_3 bulk references. (c) Same as above in the case of samples M7D and G7D.

different Fe−O bond lengths (the shorter the interatomic distance, the higher the edge energy), which gives a hint on the different oxidation state of the Fe ions (Fe^{2+} and Fe^{3+}). Consequently, the chemical sensitivity of XANES is strongly influenced by the local geometry[65,90−94] (see also the Supporting Information for further explanation).

The comparison of the Fe K-edge XANES spectra of all the studied samples, together with those of Fe_3O_4 and γ-Fe_2O_3 bulk

dx.doi.org/10.1021/jp4104992 | J. Phys. Chem. C 2014, 118, 1332−1346

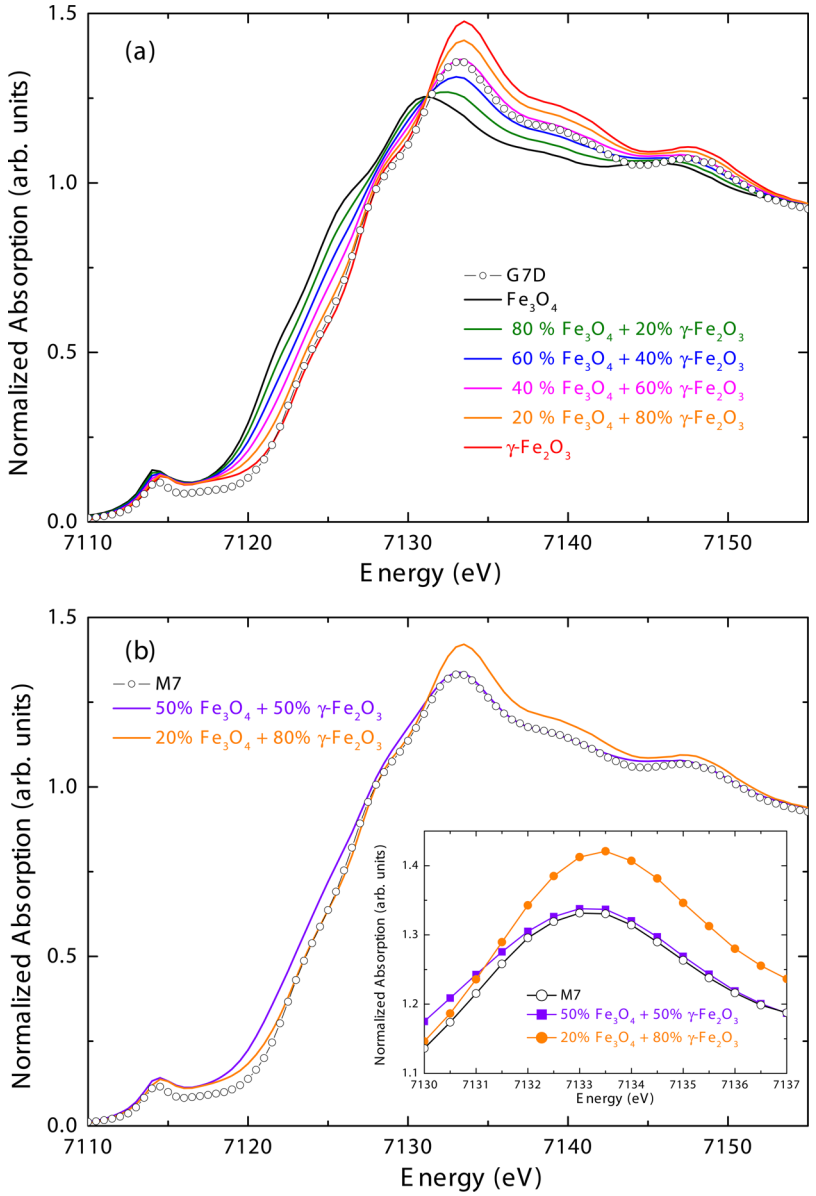

Figure 4. (a) Comparison of the experimental Fe K-edge XANES spectra of the G7D sample and the weighted sums of the experimental spectra of Fe_3O_4 and γ-Fe_2O_3 bulk references. (b) Comparison of the experimental Fe K-edge XANES spectra of the M7 sample and the weighted sums that better reproduced the edge and maximum positions, 50 and 20% of Fe_3O_4, respectively (see text for details).

references are reported in Figure 3 and in the Supporting Information (Figures 3 and 4). From these figures it is clear that none of the studied NPs display the characteristic XANES profile of bulk magnetite. The larger samples ($\phi \geq 9$ nm) display a XANES spectra intermediate between those of the magnetite and maghemite bulk references. The smaller NPs ($\phi < 9$ nm) display a XANES profile similar to that of bulk maghemite, but the white lines are less intense and reach their maximum at lower energies. We can conclude from these comparisons that none of the nanoparticles show a single-phase bulk magnetite or maghemite structure, independently of the sample synthesis method. These results are in agreement with the Fe $L_{2,3}$-edges XAS and XMCD results reported in the precedent section. This is of particular significance in the case of samples M9D and M18D for which the Fe K-edge absorption reveals significant differences, associated to a different structural arrangement. These structural effects were hindered to the Fe $L_{2,3}$-edge XAS and XMCD probes, which poses serious doubts on the reliability of the results obtained from a simple fingerprint XMCD analysis of their magnetic properties. Regarding the differences and similarities in the NPs XANES spectra, it is worth noting that all the samples with $\phi \geq 12$ nm display a XANES profile nearly identical, irrespective of the sample synthesis method or whether they undergone an extra oxidation process (see Figures 3c and Figure 4a in the Supporting Information).

Once the hypothesis of a single bulk-like phase has been disregarded, the next step is to explore the possibility of a Fe_3O_4@γ-Fe_2O_3 core−shell structure. To this end, we have checked if the NPs XANES spectra can be accounted for as a weighted sum of the experimental spectra of both Fe_3O_4 and γ-Fe_2O_3 bulk references.[95] Representative examples of these comparisons are displayed in Figures 4 and 5. As a common result we have found that none of the experimental spectra can be fully described as a linear combination of the spectra of the bulk references, that is, it is not possible to find a weighted sum

dx.doi.org/10.1021/jp4104992 | J. Phys. Chem. C 2014, 118, 1332−1346

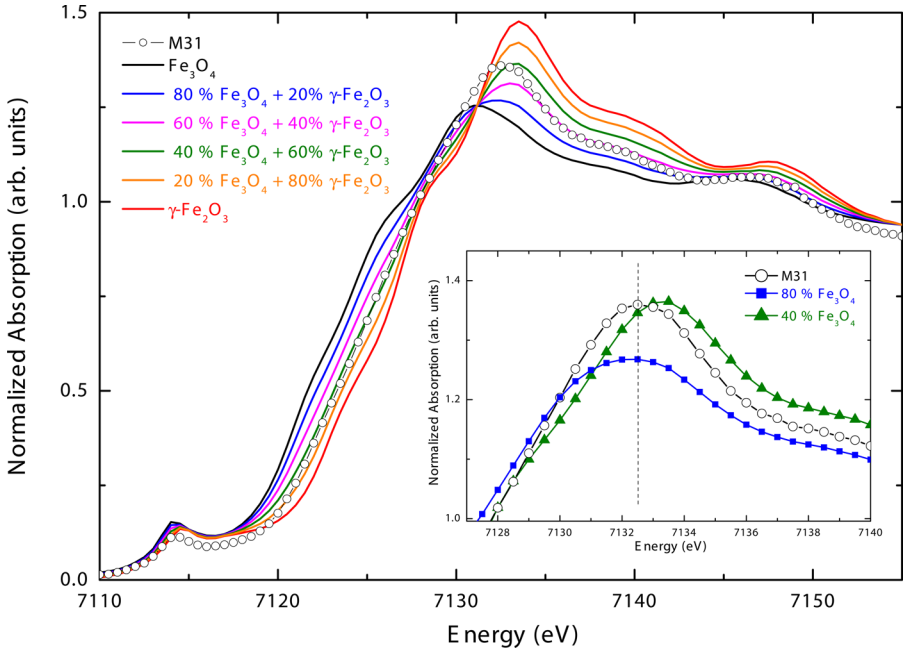

Figure 5. Comparison of the experimental Fe K-edge XANES spectra of the M31 sample and the weighted sums of the experimental spectra of Fe_3O_4 and γ-Fe_2O_3 bulk references. Inset: Comparison of the experimental Fe K-edge XANES spectra of the M31 sample and the weighted sums that better reproduced the edge and maximum positions, 40 and 80% of Fe_3O_4, respectively (see text for details).

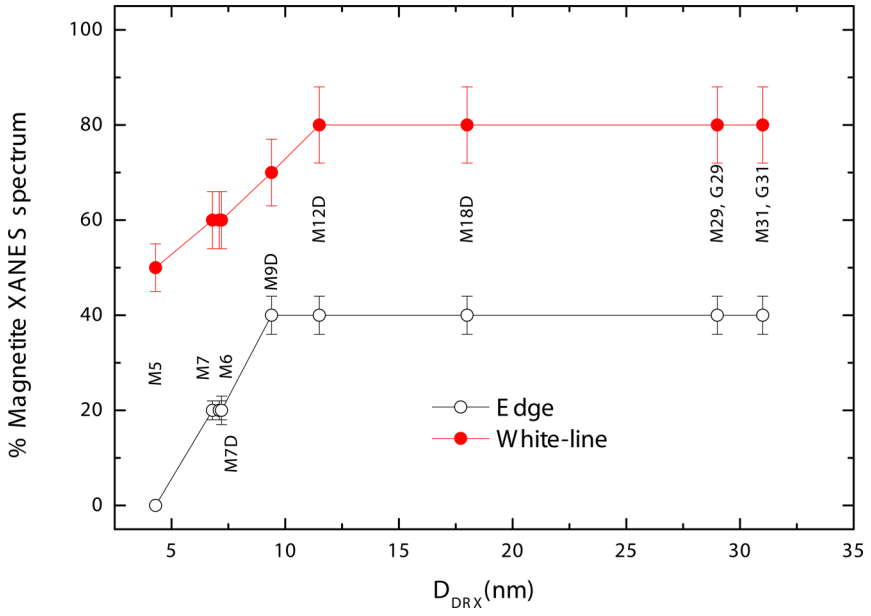

Figure 6. Dependence on the nanoparticle size of the relative amount (±5%) of magnetite XANES in the weighted sum of the experimental spectra of Fe_3O_4 and γ-Fe_2O_3 bulk references needed to match the energy position of both the edge and the white of the Fe K-edge experimental spectra (see text for details).

that simultaneously reproduces both the edge position and the white line (shape and energy position). For the smaller samples, $\phi < 9$ nm, the edge position is well reproduced by the weighted addition of the spectra in the form 10% (7%)[95] Fe_3O_4 + 90% (93%)[95] of γ-Fe_2O_3 (±10%, depending on the sample, see Figure 4). On the other hand, the best reproduction of the experimental white line region is obtained by the addition of magnetite and maghemite spectra with a relative weighting varying between 40 and 60% (30–70%) and 50 and 50% (40–60%).[95]

For the larger samples, $\phi \geq 9$ nm, see Figure 5, the edge position is well reproduced by the weighted addition 40% Fe_3O_4 + 60% γ-Fe_2O_3 (30–70%), being 50 to 50% (40–60%) for M9D; however, there is no linear combination able to reproduce the shape of the white line. A total of ∼70% of magnetite is necessary to reproduce the energy position of the maximum, but both the height and the shape of the corresponding white line are quite different from those of the experimental spectra.

These results clearly show that the NPs XANES spectra cannot be seen as a weighted sum of the experimental spectra

dx.doi.org/10.1021/jp4104992 | J. Phys. Chem. C 2014, 118, 1332–1346

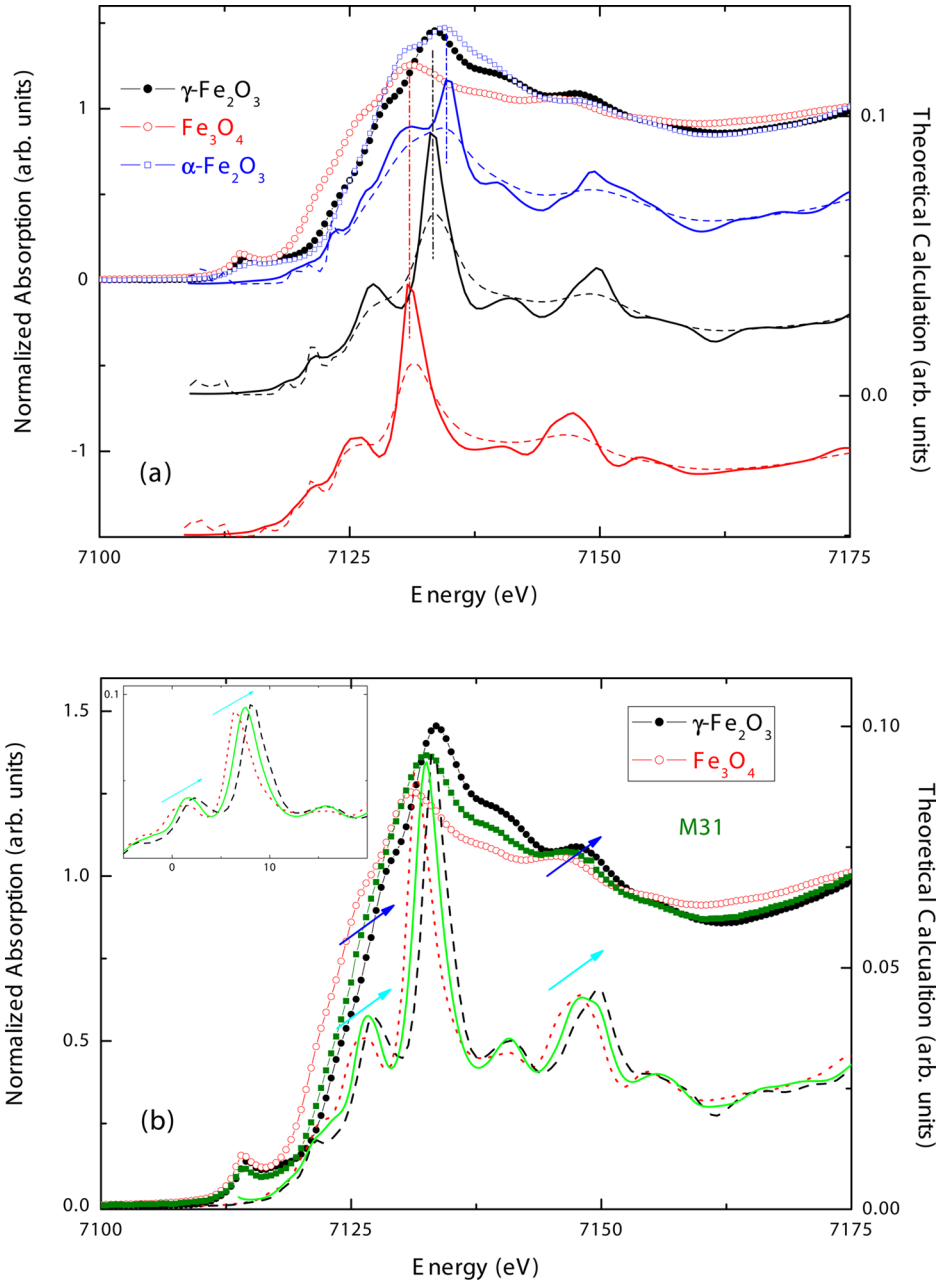

Figure 7. (a) Comparison between the experimental Fe K-edge of α-Fe_2O_3 (blue, □), Fe_3O_4 (red, ○) and γ-Fe_2O_3 (●) and the computations performed by using the Dirac-Hara ECP (solid line). The dashed lines correspond to the computations performed by using the *complex* Dirac-Hara ECP (see text for details). (b) Comparison between the experimental Fe K-edge of γ-Fe_2O_3 (●), Fe_3O_4 (red, ○), and sample M31 (green, ■), and the results of the theoretical computations performed for the original magnetite (red, dots) and maghemite (black, dash) clusters and for those (green, solid line) in which the cell parameter has been varied (see text for details). In this case only the result of the computations obtained by using the real DH are displayed in order to get an enhanced view of the differences.

of both Fe_3O_4 and γ-Fe_2O_3 bulk references. For the sake of completeness we have also studied a possible occurrence of other bulk iron oxides in the samples. However, as shown in Figure 5 of the Supporting Information, the inclusion of these antiferromagnetic phases does not significatively improve the overall spectral shape and, in particular, the white-line region.

All these results clearly indicate that the experimental spectra are not well reproduced by any linear combination of the XANES spectra of Fe_3O_4 and γ-Fe_2O_3 bulk references, even taking into account other oxides as goethite or ferrihydrite. The failure of this hypothesis reflects the inadequacy of considering the NPs as bulk-based materials, i.e. that stoichiometric bulk-like oxides can grow and coexist separately in the confined space of the NP. It should be noted in this respect that the present results cast serious doubts regarding the gradual increase of the magnetite content as the particle size does in the proposed magnetite-maghemite core−shell model. As shown in Figure 6, the relative amount of magnetite needed to account for the edge or white-line position of the Fe K-edge spectra of nanoparticles of increasing size "saturates" for $\phi \geq 12$ nm, while a linear increase is expected according to the magnetite−maghemite core−shell model.

The fact that the XAS spectrum remains basically invariable for NPs with $\phi \geq 12$ nm implies that the local structural

dx.doi.org/10.1021/jp4104992 | J. Phys. Chem. C 2014, 118, 1332−1346

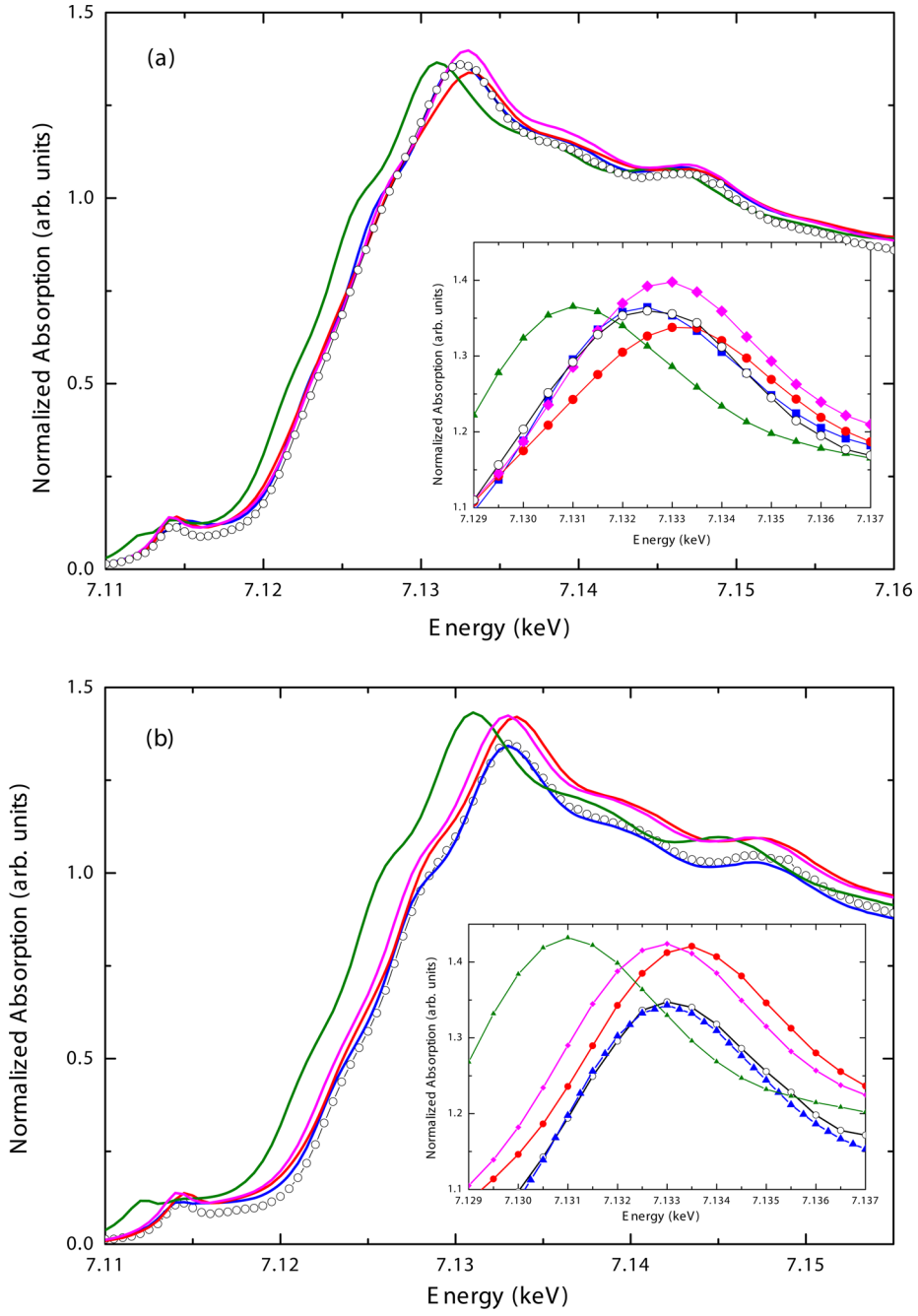

Figure 8. (a) Fe K-edge XANES spectra of M31 (○) together the best fit obtained with the weighted sums of the displaced references: 50% Fe_3O_4 + 50% γ-Fe_2O_3 (red, ●), 50% Fe_3O_4 (ΔE = 1 eV) + 50% γ-Fe_2O_3 (ΔE = −1 eV) (blue, ■), 50% Fe_3O_4 + 50% γ-Fe_2O_3 (ΔE = −2.5 eV) (green, ▲), 30% Fe_3O_4 + 70% γ-Fe_2O_3 (ΔE = −0.5 eV) (magenta, ◆). (b) Same as above in the case of the M4 sample (black, ○): 20% Fe_3O_4 + 80% γ-Fe_2O_3 (red, ●), 20% Fe_3O_4 (ΔE = 1 eV) + 80% γ-Fe_2O_3 (ΔE = −1 eV) (blue, ▲), 20% Fe_3O_4 + 80% γ-Fe_2O_3 (ΔE = −2.5 eV) (green, ▲), 20% Fe_3O_4+ 80% γ-Fe_2O_3 (ΔE = −0.5 eV) (magenta, ◆).

arrangement of Fe does not depend on the NPs size, as expected for a core/shell scheme, and supports the existence of a single nonstoichiometric phase. Similarly, our results show that for a given particle size, see for instance M7 versus M7D, the local structural arrangement of Fe depends little on the synthesis method (in principle, affecting the oxidation rate). It should be noted in this respect that, within the core−shell scenario, samples obtained by thermal decomposition should exhibit, in principle, a greater content of magnetite because the reaction is carried out in organic media in the presence of hexadecanediol[96] and the oleic acid prevents from oxidation.[54] Similarly, for those samples subjected to further oxidation, a majority maghemite phase should be expected, contrary to the experimental results. All these results suggest that a single phase is developed inside the NPs during the synthesis process. This phase is unaffected by further oxidation processes and its structural details are mainly determined by steric effects; that is, the partial oxidation of the nominal magnetite NPs mainly comes from a larger disorder on the octahedral subnetwork, allowing the appearance of vacancies in the spinel octahedral sites. This disorder, caused by the size constraint, leads to the modification of the structural arrangements at the Fe sites with

dx.doi.org/10.1021/jp4104992 | J. Phys. Chem. C 2014, 118, 1332−1346

respect to those found in bulk-like iron oxides. This new, intermediate phase can be seen as a mixture of "structurally adapted" magnetite and maghemite oxides in such a way that magnetite and maghemite rearrange their crystallographic structure in order to get the same crystal cell parameter, being the size of the NPs that determines the variation of the parameter cell and the distribution of the vacancies. Hence, we have explored the possibility that the formed Fe oxide grows in a single crystal structure with a cell parameter lying in between those of the pure stoichiometric magnetite and maghemite oxides. Because no reference spectra exist for this purpose, we have investigated this possibility with ab initio theoretical calculations of the Fe K-edge XANES.

Initially, we have performed the computations for the bulk-like structures. The result of the calculations performed for the reference bulk oxides are shown Figure 7 (see the Supporting Information for computational details). In all cases, the computations reproduce not only the overall experimental spectral shape, but also the relative intensity of the spectral features, as well as their relative energy separation. In addition, computations displayed on an unique energy scale reproduce the characteristic edge shift associated to the different interatomic distances of these oxides.

We have explored in a second step the possibility that the formed Fe oxide grows in a single crystal structure with a cell parameter lying in between those of the pure stoichiometric magnetite and maghemite oxides. If this is the case not only the structural arrangements at the Fe sites but also the distribution of the Fe^{2+} and Fe^{3+} ions, including vacancies, would slightly depart from those of bulk Fe_3O_4 and γ-Fe_2O_3 stoichiometric iron oxides. Therefore we have performed the calculations by considering it as an intermediate structure between Fe_3O_4 and γ-Fe_2O_3. To this end we have carried out the same class of computations for Fe_3O_4 and γ-Fe_2O_3 clusters in which the cell parameter have been progressively modified up to reach 8.364 Å, that is, the average of those of the pure magnetite and maghemite compounds. The modification of the cell parameter leads to the overall shift of the spectra without modifying the spectral shape. When decreasing the cell parameter of Fe_3O_4, that is, the Fe−O interatomic distance, the main absorption peak shifts to higher energies, while the contrary occurs for γ-Fe_2O_3 in which the cell parameter is being increased. As a result, when the computation is performed for both magnetite and maghemite clusters by imposing the same (averaged) cell parameter, the main peak lies in the middle between those of the unmodified clusters. Figure 7b shows the comparison of the computations performed for the original magnetite and maghemite clusters and the 50% weighted sum[97] of the spectra computed for the clusters modified as detailed above. The results are compared to the experimental spectra of both bulk Fe_3O_4 and γ-Fe_2O_3 and of representative M31 sample. The computations reproduce both the experimental energy shift of the different spectral features as well as the relative variation of the intensity of the main absorption line. The good agreement between the experimental and theoretical spectra strongly supports that the Fe oxide grows in the NPs as a single spinel structure whose structural parameters and Fe^{2+}/Fe^{3+} ratio differs form those of bulk magnetite and maghemite.

Finally, we have taken advantage of the results of the theoretical computations to apply a similar procedure to the experimental spectra. In this way we have applied the weighting procedure of the XANES spectra of the bulk magnetite and maghemite references but shifting their energy scale prior addition, that is, simulating to some extent their expected variation upon modification of the structural parameters.[97] The comparison to the experimental spectra, reported in Figure 8, shows an excellent agreement among the experimental spectra and the calculated ones. In the case of the larger samples, good agreement is obtained by a 50% weighting of the Fe_3O_4 and γ-Fe_2O_3 after shifting them by $\Delta E = \pm 0.75$ or ± 1 eV. As discussed above, this procedure is an empirical way of taking into account the modification of the interatomic distances. Provided that the cell parameters of magnetite and maghemite are 8.394 and 8.334 Å, respectively, the positive shift applies for magnetite, that is, decreasing the Fe−O distance, and the negative to maghemite, that is, increasing the bond length. In the case of the smaller samples, the best fit is obtained by applying a $\Delta E = 1.5$ eV for magnetite reference spectra and $\Delta E = -0.5$ eV for the maghemite one, which agrees with the fact that the experimental edge position (and, consequently, the bond length) is closer to maghemite. As a final test, we have also considered the possibility of a core−shell arrangement where the core corresponds to bulk-like magnetite and the shell to "oxidized" (modified cell parameter) magnetite. In this case, the weighting of the reference spectra should be made without shifting the energy of the Fe_3O_4 one. No good agreement with the experimental spectra is obtained by following this procedure.

The results obtained in this work support the existence of a single "nonstoichiometric" phase in these nominal magnetite nanoparticles. None of the nanoparticles show a single-phase bulk magnetite or maghemite structure, independent of the sample synthesis method. Moreover, the XAS spectra cannot be accounted for in terms of a mixture of bulk-like iron oxides. The fact that no modification of the Fe K-edge XANES is observed between samples grown by different procedures (including extra oxidation) suggests that the local structural arrangement of Fe and, therefore, its related structural disorder, depends mainly on the NPs size. This dependence would not be linear, but range-defined. In other words, the particle size plays the main role in determining the structural properties of the NPs, the modification of the interatomic distances, the ratio of Fe ions in different electronic state, and the crystal field parameters, which in turn determine other properties.

SUMMARY AND CONCLUSIONS

In this work we propose a new approach to determine the structure of Fe oxide NPs by using the Fe K-edge X-ray absorption near edge spectroscopy. To this end, we have performed a detailed XANES study at the Fe K- and $L_{2,3}$-edges on nominal magnetite nanoparticles synthesized by different methods. In addition, X-ray magnetic circular dichroism was recorded at the Fe $L_{2,3}$-edges in selected samples. Our main objective is to determine if the nominal Fe_3O_4 nanoparticles are single or multiphase systems, as well as the nature of these phases.

We have verified that the Fe $L_{2,3}$-edge absorption alone is not able to determine the structure of nanosized magnetite NPs. As far as the Fe $L_{2,3}$-edge absorption is dictated by the valence and point symmetry of the absorbing sites, the overall line shape of all the iron oxides is similar, making complicated to identify the relative amount of the oxide phases present in the material. In contrast, the Fe K-edge spectral shape is clearly different for all the references considered, reflecting the high sensitivity of the Fe K-edge absorption to the geometrical details of the absorbing site. Another critical advantage of using the Fe K-

dx.doi.org/10.1021/jp4104992 | J. Phys. Chem. C 2014, 118, 1332−1346

edge absorption for this purpose is that it probes the whole NPs, whereas the probing depth of the Fe $L_{2,3}$-edge absorption is only ~45 Å in iron oxides, which limits its accuracy to evaluate possible surface/volume effects.

The analysis of the XAS data recorded at both Fe K- and $L_{2,3}$-edges indicates that the experimental spectra are not well reproduced by any linear combination of the absorption spectra of Fe_3O_4 and γ-Fe_2O_3 bulk references, even taking into account other oxides as goethite or ferrihydrite. In other words, none of the synthesized NPs can be identified as a mixture of stoichiometric bulk-like iron oxides, independent of the sample synthesis method or whether they undergo an extra oxidation process. The failure of this hypothesis reflects the inadequacy of considering the NPs as bulk-based materials, that is, that stoichiometric bulk-like oxides can grow and coexist separately in the confined space of the NP.

The analysis of the Fe K-edge spectra indicates that the local structural arrangement of Fe does not depend on the NPs size, as expected for a core/shell scheme. Likewise, we can conclude that the local structural arrangement of Fe is very stable and it depends little on the synthesis method (in principle, affecting the oxidation rate) and that it does not change when the NPs are subjected to a further oxidation (in this case, a majority maghemite phase should be expected, contrary to the experimental results). Moreover, our results indicate that the synthesis of the Fe_3O_4 magnetite nanoparticles leads to the growing of a single phase nonstoichiometric oxide whose crystal structure possesses a cell parameter lying in between those of the pure stoichiometric magnetite and maghemite oxides.

■ ASSOCIATED CONTENT

Supporting Information

XRD patterns and TEM images of samples synthesized by different methods. Additional XAS data and details of the ab initio XANES calculations. This material is available free of charge via the Internet at http://pubs.acs.org.

■ AUTHOR INFORMATION

Corresponding Author

*E-mail: jchaboy@unizar.es.

Present Addresses

[§]Catalonian Institute of Nanotechnology (ICN), UAB Campus, E-08193 Bellaterra (Barcelona), Spain (A.G.R.).

[∥]Diamond Light Source Ltd., Harwell Science and Innovation Campus, Chilton, Didcot, Oxfordshire, OX11 0DE, U.K. (R.B.).

Notes

The authors declare no competing financial interest.

■ ACKNOWLEDGMENTS

This work was partially supported by Spanish MAT2010-09346-E, MAT2010-16022, and MAT2011-27573-C04-04, and by the Aragón DGA NETOSHIMA Grant. The synchrotron radiation experiments were performed at APS and at SPring-8 (Prop. Num. 2012A0024). Use of the Advanced Photon Source, an Office of Science User Facility operated for the U.S. Department of Energy (DOE) Office of Science by Argonne National Laboratory, was supported by the U.S. DOE under Contract No. DE-AC02-06CH11357. We acknowledge R. Rosenberg for his assistance during the SR experiments at APS. We acknowledge J. Blasco and G. Subías for supplying us the bulk magnetite reference sample,[98] and to F. Balas and A. Clemente for helpful discussions. C.G. acknowledges the Ministerio de Eduación y Ciencia of Spain for a Ph.D. Grant. M.A.L.-M. acknowledges CSIC for a JAE-Doc contract within the *Junta para la Ampliación de Estudios* program. C.P. and A.G.R. thanks support from CSIC (Research Project 200980I05) and R.B. from the Ministerio de Economía y Competitividad of Spain.

■ REFERENCES

(1) Tartaj, P. Nanomagnets-From Fundamental Physics to Biomedicine. *Curr. Nanosci.* **2006**, *2*, 43−53.

(2) Berry, C. C.; Curtis, A. S. G. Functionalisation of Magnetic Nanoparticles for Applications in Biomedicine. *J. Phys. D: Appl. Phys.* **2003**, *36*, R198−R206.

(3) Gutiérrez, L.; Lázaro, A. R.; Abadía, F. J.; Romero, C.; Quintana, M. S.; Morales, M. P.; Patiño, C.; Arranz, R. Bioinorganic Transformations of Liver Iron Deposits Observed by Tissue Magnetic Characterisation in a Rat Model. *J. Inorg. Biochem.* **2006**, *100*, 1790−1799.

(4) Morales, M. P.; Veintemillas-Verdaguer, S.; Montero, M. I.; Serna, C. J.; Roig, A.; Casas, L.; Martínez, B.; Sandiumenge, F. Surface and Internal Spin Canting in γ-Fe_2O_3 Nanoparticles. *Chem. Mater.* **1999**, *11*, 3058−3064.

(5) Tartaj, P.; Morales, M. P.; Veintemillas-Verdaguer, S.; González-Carreño, T.; Serna, C. J. The Preparation of Magnetic Nanoparticles for Applications in Biomedicine. *J. Phys. D: Appl. Phys.* **2003**, *36*, R182−R197.

(6) Demortiere, A.; Panissod, P.; Pichon, B. P.; Pourroy, G.; Guillon, D.; Donnio, B.; Begin-Colin, S. Size-Dependent Properties of Magnetic Iron Oxide Nanocrystals. *Nanoscale* **2011**, *3*, 225−232.

(7) Gorski, C. A.; Scherer, M. M. Determination of Nanoparticulate Magnetite Stoichiometry by Mössbauer Spectroscopy, Acidic Dissolution, and Powder X-ray Diffraction: A Critical Review. *Am. Mineral.* **2010**, *95*, 1017−1026.

(8) Latta, D. E.; Gorski, C. A.; Boyanov, M. I.; O'Loughlin, E. J.; Kemner, K. M.; Scherer, M. M. Influence of Magnetite Stoichiometry on U^{VI} Reduction. *Environ. Sci. Technol.* **2012**, *46*, 778−786.

(9) Lilova, K.; Xu, F.; Rosso, K.; Pearce, C.; Kamali, S.; Navrotsky, A. Oxide Melt Solution Calorimetry of Fe^{2+}-Bearing Oxides and Application to the Magnetite-Maghemite (Fe_3O_4-$Fe_{8/3}O_4$) System. *Am. Mineral.* **2011**, *97*, 164−175.

(10) Morup, S. Mössbauer Spectroscopy Studies of Suspensions of Fe_3O_4 Microcrystals. *J. Magn. Magn. Mater.* **1983**, *39*, 45−47.

(11) da Costa, G. M.; de Grave, E.; de Bakker, P. M. A.; Vandenberghe, R. E. Influence on Nonstoichiometry and the Presence of Maghemite on the Mössbauer Spectrum of Magnetite. *Clays Clay Miner.* **1995**, *43*, 656−668.

(12) Billinge, S. J. L.; Levin, I. The Problem with Determining Atomic Structure at the Nanoscale. *Science* **2007**, *316*, 561−565.

(13) Topsøe, H.; Dumesic, J. A.; Boudart, M. Mössbauer Spectra of Stoichiometric and Nonstoichiometric Fe_3O_4 Microcrystals. *J. Phys. (Paris) Colloq.* **1974**, *35* (C6), 411−413.

(14) Haneda, K.; Morrish, A. H. Magnetite to Maghemite Transformation in Ultrafine Particles. *J. Phys. (Paris) Colloq.* **1977**, *38* (Cl), 321−323.

(15) Jubb, A. M.; Allen, H. C. Vibrational Spectroscopic Characterization of Hematite, Maghemite, and Magnetite Thin Films Produced by Vapor Deposition. *ACS Appl. Mater. Interfaces* **2010**, *2*, 2804−2812.

(16) Li, Y.-S.; Church, J. S.; Woodhead, A. L. Infrared and Raman Spectroscopic Studies on Iron Oxide Magnetic Nano-particles and their Surface Modifications. *J. Magn. Magn. Mater.* **2012**, *324*, 1543−1550.

(17) Slavov, L.; Abrashev, M.; Merodiiska, T.; Gelev, C.; Vandenberghe, R.; Markova-Deneva, I.; Nedkov, I. Raman Spectroscopy Investigation of Magnetite Nanoparticles in Ferrofluids. *J. Magn. Magn. Mater.* **2010**, *322*, 1904−1911.

(18) de Faria, D. L. A.; Silva, S. V.; de Oliveira, M. T. Raman Microspectroscopy of Some Iron Oxides and Oxyhydroxides. *J. Raman Spectrosc.* **1997**, *28*, 873−878.
(19) Oblonsky, L. J.; Devine, T. M. A Surface Enhanced Raman Spectroscopic Study of the Passive Films Formed in Borate Buffer on Iron, Nickel, Chromium and Stainless Steel. *Corros. Sci.* **1995**, *37*, 17−41.
(20) Feitknecht, W.; Gallagher, K. J. Mechanisms for the Oxidation of Fe_3O_4. *Nature* **1970**, *228*, 548−549.
(21) Gallagher, K. J. Mechanism of Oxidation of Magnetite to γ-Fe_2O_3. *Nature* **1968**, *217*, 1118−1121.
(22) Shebanova, O. N.; Lazor, P. Raman Study of Magnetite (Fe_3O_4): Laser Induced Thermal Effects and Oxidation. *J. Raman Spectrosc.* **2003**, *34*, 845−852.
(23) Sidhu, P. S. Transformation of Trace Element-Substituted Maghemite to Hematite. *Clays Clay Miner.* **1988**, *36*, 31−38.
(24) Farrel, D. M., Ed. In *A Study of the Oxidation of Magnetite or Ferrosoferric Oxide*; University of Ottawa: Canada, 1973; http://ruor.uottawa.ca/en/handle/10393/7090.
(25) van Aken, P. A.; Liebscher, B. Quantification of Ferrous/Ferric Ratios in Minerals: New Evaluation Schemes of Fe $L_{2,3}$ Electron Energy-Loss Near-Edge Spectra. *Phys. Chem. Miner.* **2002**, *29*, 188−200.
(26) van Aken, P. A.; Liebscher, B.; Styrsa, V. J. Quantitative Determination of Iron Oxidation States in Minerals Using Fe $L_{2,3}$-Edge Electron Energy-Loss Near-Edge Structure Spectroscopy. *Phys. Chem. Miner.* **1998**, *25*, 323−327.
(27) van der Laan, G.; Kirkman, I. W. The 2p Absorption Spectra of 3d Transition Metal Compounds in Tetrahedral and Octahedral Symmetry. *J. Phys.: Condens. Matter* **1992**, *4*, 4189−4204.
(28) Crocombette, J. P.; Pollak, M.; Jollet, F.; Thromat, N.; Gautier-Soyer, M. X-ray Absorption Spectroscopy at the Fe $L_{2,3}$ Threshold in Iron Oxides. *Phys. Rev. B* **1995**, *52*, 3143−3150.
(29) Park, J.; An, K.; Hwang, Y.; Park, J.-G.; Noh, H.-J.; Kim, J.-Y.; Park, J.-H.; Hwang, N.-M.; Hyeon, T. Ultra-Large-Scale Syntheses of Monodisperse Nanocrystals. *Nat. Mater.* **2004**, *3*, 891−895.
(30) Jeng, H.-T.; Guo, G. Y. First-Principles Investigations of the Electronic Structure and Magnetocrystalline Anisotropy in Strained Magnetite Fe_3O_4. *Phys. Rev. B* **2002**, *65*, 094429/1−9.
(31) Brice-Profeta, S.; Arrio, M.-A.; Tronc, E.; Menguy, N.; Letard, I.; dit Moulin, C. C.; Nogués, M.; Chaneac, C.; Jolivet, J.-P.; Sainctavit, P. Magnetic Order in γ-Fe_2O_3 Nanoparticles: a XMCD Study. *J. Magn. Magn. Mater.* **2005**, *288*, 354−365.
(32) Goering, E.; Lafkioti, M.; Gold, S. Comment on "Spin and Orbital Magnetic Moments of Fe_3O_4. *Phys. Rev. Lett.* **2006**, *96*, 039701.
(33) Huang, D. J.; Chang, C. F.; Jeng, H.-T.; Guo, G. Y.; Lin, H.-J.; Wu, W. B.; Ku, H. C.; Fujimori, A.; Takahashi, Y.; Chen, C. T. Spin and Orbital Magnetic Moments of Fe_3O_4. *Phys. Rev. Lett.* **2004**, *93*, 077204/1−4.
(34) Yamasaki, A.; Kobori, H.; Osawa, H.; Nakamura, T.; Sugimura, A. Soft X-ray Magnetic Circular Dichroism Study of Magnetite Nanoparticles. *J. Phys.: Confer. Ser.* **2009**, *150*, 042235/1−4.
(35) Pérez, N.; Bartolomé, F.; García, L. M.; Bartolomé, J.; Morales, M. P.; Serna, C. J.; Labarta, A.; Batlle, X. Nanostructural Origin of the Spin and Orbital Contribution to the Magnetic Moment in $Fe_{3-x}O_4$ Magnetite Nanoparticles. *Appl. Phys. Lett.* **2009**, *94*, 093108/1−3.
(36) Roca, A. G.; Marco, J. F.; Morales, M. d. P.; Serna, C. J. Effect of Nature and Particle Size on Properties of Uniform Magnetite and Maghemite Nanoparticles. *J. Phys. Chem. C* **2007**, *111*, 18577−18584.
(37) Signorini, L.; Pasquini, L.; Savini, L.; Carboni, R.; Boscherini, F.; Bonetti, E.; Giglia, A.; Pedio, M.; Mahne, N.; Nannarone, S. Size-Dependent Oxidation in Iron/Iron Oxide Core-Shell Nanoparticles. *Phys. Rev. B* **2003**, *68*, 195423/1−8.
(38) Santoyo Salazar, J.; Perez, L.; de Abril, O.; Truong Phuoc, L.; Ihiawakrim, D.; Vazquez, M.; Greneche, J.-M.; Begin-Colin, S.; Pourroy, G. Magnetic Iron Oxide Nanoparticles in 10−40 nm Range: Composition in Terms of Magnetite/Maghemite Ratio and Effect on the Magnetic Properties. *Chem. Mater.* **2011**, *23*, 1379−1386.
(39) Kaiser, R.; Miskolczy, G. Magnetic Properties of Stable Dispersions of Subdomain Magnetite Particles. *J. Appl. Phys.* **1970**, *41*, 1064−1072.
(40) Sarkar, D.; Mandal, M. Static and Dynamic Magnetic Characterization of DNA-Templated Chain-Like Magnetite Nanoparticles. *J. Phys. Chem. C* **2012**, *116*, 3227−3234.
(41) Gangopadhyay, S.; Hadjipanayis, G. C.; Dale, B.; Sorensen, C. M.; Klabunde, K. J.; Papaefthymiou, V.; Kostikas, A. Magnetic Properties of Ultrafine Iron Particles. *Phys. Rev. B* **1992**, *45*, 9778−9787.
(42) Goya, G. F.; Berquo, T. S.; Fonseca, F. C.; Morales, M. P. Static and Dynamic Magnetic Properties of Spherical Magnetite Nanoparticles. *J. Appl. Phys.* **2003**, *94*, 3520−3528.
(43) Wilke, M.; Farges, F.; Pettit, P.-M.; Brown, G. E., Jr.; Martins, F. Oxidation State and Coordination of Fe in Minerals: An Fe K-XANES Spectroscopic Study. *Am. Mineral.* **2001**, *86*, 714−730.
(44) O'Day, P. A.; Rivera, N., Jr.; Root, R.; Carroll, S. A. X-ray Absorption Spectroscopic Study of Fe Reference Compounds for the Analysis of Natural Sediments. *Am. Mineral.* **2004**, *89*, 572−585.
(45) Berry, A. J.; Yaxley, G. M.; Woodland, A. B.; Foran, G. J. A XANES Calibration for Determining the Oxidation State of Iron in Mantle Garnet. *Chem. Geol.* **2010**, *278*, 31−37.
(46) Pellegrin, E.; Hagelstein, M.; Doyle, S.; Moser, H. O.; Fuchs, J.; Vollath, D.; Schuppler, S.; James, M. A.; Saxena, S. S.; Niesen, L.; et al. Characterization of Nanocrystalline γ-Fe_2O_3 with Synchrotron Radiation Techniques. *Phys. Status Solidi B* **1999**, *215*, 797−801.
(47) Corrias, A.; Ennas, G.; Mountjoy, E.; Paschina, G. An X-ray Absorption Spectroscopy Study of the Fe K edge in Nanosized Maghemite and in Fe_2O_3-SiO_2 Nanocomposites. *Phys. Chem. Chem. Phys.* **2000**, *2*, 1045−1050.
(48) Waychunas, G. A.; Apted, M. J.; Brown, G. E., Jr. X-Ray K-Edge Absorption Spectra of Fe Minerals and Model Compounds: Near-Edge Structure. *Phys. Chem. Miner.* **1983**, *10*, 1−9.
(49) Benfatto, M.; Solera, J. A.; García, J.; Chaboy, J. Double-Channel Excitation in the X-ray Absorption Spectrum of Fe^{3+} Water Solutions. *Chem. Phys.* **2002**, *282*, 441−450.
(50) Okudera, H.; Yoshiasa, A.; Murai, K.; Okube, M.; Takeda, T.; Kikkawa, S. Local Structure of Magnetite and Maghemite and Chemical Shift in Fe K-edge XANES. *J. Miner. Petrol. Sci.* **2012**, *107*, 127−132.
(51) Espinosa, A.; Serrano, A.; Llavona, A.; Jimenez de la Morena, J.; Abuin, M.; Figuerola, M.; Pellegrino, T.; Fernández, J. F.; García-Hernández, M.; Castro, G. R.; et al. On the Discrimination between Magnetite and Maghemite by XANES Measurements in Fluorescence Mode. *Meas. Sci. Technol.* **2012**, *23*, 015602/1−6.
(52) Gota, S.; Gautier-Soyer, M.; Sacchi, M. Fe 2*p* Absorption in Magnetic Oxides: Quantifying Angular-Dependent Saturation Effects. *Phys. Rev. B* **2000**, *62*, 4187−4190.
(53) Gupta, A. K.; Gupta, M. Synthesis and Surface Engineering of Iron Oxide Nanoparticles for Biomedical Applications. *Biomaterials* **2005**, *26*, 3995−4021.
(54) Roca, A. G.; Morales, M. P.; O'Grady, K.; Serna, C. J. Structural and Magnetic Properties of Uniform Magnetite Nanoparticles prepared by High Temperature Decomposition of Organic Precursors. *Nanotechnology* **2006**, *17*, 2783−2788.
(55) Andres-Vergés, M.; Costo, R.; Roca, A. G.; Marco, J. F.; Goya, G. F.; Serna, C. J.; Morales, M. P. Uniform and Water Stable Magnetite Nanoparticles with Diameters around the Monodomain-Multidomain Limit. *J. Phys. D: Appl. Phys.* **2008**, *41*, 134003/1−10.
(56) Massart, R.; Cabuil, V. Effect of Some Parameters on the Formation of Colloidal Magnetite in Alkaline Medium: Yield and Particle-Size Control. *J. Chem. Phys.* **1987**, *84*, 967−973.
(57) Laurent, S.; Forge, D.; Port, M.; Roch, A.; Robic, C.; Vanderelst, L.; Muller, R. N. Magnetic Iron Oxide Nanoparticles: Synthesis, Stabilization, Vectorization, Physicochemical Characterizations, and Biological Applications. *Chem. Rev.* **2008**, *108*, 2064−2110.
(58) Li, Z.; Tan, B.; Allix, M.; Cooper, A. I.; Rosseinsky, M. J. Direct Coprecipitation Route to Monodisperse Dual-Functionalized Mag-

netic Iron Oxide Nanocrystals without Size Selection. *Small* **2008**, *4*, 231−239.
(59) Roca, A. G.; Morales, M. P.; Serna, C. J. Synthesis of Monodispersed Magnetite Particles from Different Organometallic Precursors Magnetics. *IEEE Trans. Magn.* **2006**, *42*, 3025−3029.
(60) Sayers, D. E.; Bunker, B. A. In *X-Ray Absorption: Principles, Applications, Techniques of EXAFS, SEXAFS, and XANES*; Koningsberger, D. C., Prins, R., Eds.; Wiley: New York, 1988; Chapter 6.
(61) Ravel, B.; Newville, M. ATHENA, ARTEMIS, HEPHAESTUS: Data Analysis for X-ray Absorption Spectroscopy Using IFEFFIT. *J. Synchrotron Radiat.* **2005**, *12*, 537−541.
(62) Natoli, C. R.; Misemer, D. R.; Doniach, S.; Kutzler, F. W. First Principle Calculation of X-ray Absorption Edge Structure in Molecular Clusters. *Phys. Rev. A* **1980**, *22*, 1104−1108.
(63) Benfatto, M.; Longa, S. D. Geometrical Fitting of Experimental XANES Spectra by a Full Multiple-Scattering Procedure. *J. Synchrotron Radiat.* **2001**, *8*, 1087−1094.
(64) Chaboy, J.; Quartieri, S. X-ray Absorption at the Ca K-edge in Natural Garnets Solid Solutions: a Full Multiple-Scattering Investigation. *Phys. Rev. B* **1995**, *52*, 6349−6357.
(65) Chaboy, J. Relationship between the Structural Distortion and the Mn Electronic State in $La_{1-x}Ca_xMnO_3$: a Mn K -edge XANES Study. *J. Synchrotron Radiat.* **2009**, *16*, 533−544.
(66) Chaboy, J.; Muñoz-Páez, A.; Carrera, F.; Merkling, P.; Sánchez Marcos, E. Ab Initio X-ray Absorption Study of Copper K-edge XANES Spectra in Cu(II) Compounds. *Phys. Rev. B* **2005**, *71*, 134208/1−7.
(67) Chaboy, J.; Maruyama, H.; Kawamura, N. Ab Initio X-ray Absorption Study of Mn K-edge XANES Spectra in Mn_3MC (M = Sn, Zn, and Ga) Compounds. *J. Phys.: Condens. Matter* **2007**, *19*, 216214/1−9.
(68) Chaboy, J.; Nakajima, N.; Tezuka, Y. Ab initio X-ray Absorption Near-Edge Structure Study of Ti K-Edge in Rutile. *J. Phys.: Condens. Matter* **2007**, *19*, 266206/1−9.
(69) Guglieri, C.; Chaboy, J. Characterization of the ZnO-ZnS Interface in THIOL-Capped ZnO Nanoparticles Exhibiting Anomalous Magnetic Properties. *J. Phys. Chem. C* **2010**, *114*, 19629−19634.
(70) Wu, Z. Y.; Xian, D. C.; Hu, T. D.; Xie, Y. N.; Tao, Y.; Natoli, C. R.; Paris, E.; Marcelli, A. Quadrupolar Transitions and Medium-Range-Order Effects in Metal K-Edge X-ray Absorption Spectra of 3d transition-metal compounds. *Phys. Rev. B* **2004**, *70*, 033104/1−4.
(71) Guglieri, C.; Céspedes, E.; Prieto, C.; Chaboy, J. X-ray Absorption Study of the Local Order around Mn in Mn:ZnO Thin Films: the Role of Vacancies and Structural Distortions. *J. Phys.: Condens. Matter* **2011**, *23*, 206006/1−8.
(72) Díaz-Moreno, S.; Muñoz-Páez, A.; Chaboy, J. X-ray Absorption Spectroscopy (XAS) Study of the Hydration Structure of Yttrium(III) Cations in Liquid and Glassy States: Eight- or Nine-Fold Coordination? *J. Phys. Chem. A* **2000**, *104*, 1278−1286.
(73) Díaz-Moreno, S.; Chaboy, J. Ab Initio X-ray Absorption Spectroscopy Study of the Solvation Structure of Yttrium(III) in Dimethyl Sulfoxide. *J. Phys. Chem. B* **2009**, *113*, 3527−3535.
(74) Chaboy, J.; Díaz-Moreno, S. Ab Initio X-ray Absorption Spectroscopy Study of the Solvation Structure of Th(IV), U(IV), and Np(IV) in Aqueous Solution. *J. Phys. Chem. A* **2011**, *115*, 2345−2349.
(75) Krause, M. O.; Oliver, J. H. Natural Widths of Atomic K and L Levels, Kα X-ray Lines and Several KLL Auger Lines. *J. Phys. Chem. Ref. Data* **1979**, *8*, 329−338.
(76) Kim, D. H.; Lee, H. J.; Kim, G.; Koo, Y. S.; Jung, J. H.; Shin, H. J.; Kim, J.-Y.; Kang, J.-S. Interface Electronic Structures of $BaTiO_3$X Nanoparticles (X = γ-Fe_2O_3, Fe_3O_4, α-Fe_2O_3, and Fe) Investigated by XAS and XMCD. *Phys. Rev. B* **2009**, *79*, 033402/1−4.
(77) Chang, L.; Pattrick, R. A. D.; van der Laan, G.; Coker, V. S.; Roberts, A. P. Enigmatic X-ray Magnetic Circular Dichroism in Greigite (Fe_3S_4). *Can. Mineral.* **2012**, *50*, 667−674.
(78) Carvallo, C.; Sainctavit, P.; Arrio, M.-A.; Menguy, N.; Wang, Y.; Ona-Nguema, G.; Brice-Profeta, S. Biogenic versus Abiogenic Magnetite Nanoparticles: a XMCD Study. *Am. Mineral.* **2008**, *93*, 880−885.
(79) van der Laan, G.; Thole, B. T. Strong Magnetic-X-ray Dichroism in 2p Absorption-Spectra of 3d Transition-Metal Ions. *Phys. Rev. B* **1991**, *43*, 13401−13411.
(80) Pattrick, R. A. D.; van der Laan, G.; Henderson, C. M. B.; Kuiper, P.; Dudzik, E.; Vaughan, D. J. Cation Site Occupancy in Spinel Ferrites Studied by X-ray Magnetic Circular Dichroism: Developing a Method for Mineralogists. *Eur. J. Mineral.* **2002**, *14*, 1095−1102.
(81) Schedin, F.; Hill, E. W.; van der Laan, G.; Thornton, G. Magnetic Properties of Stoichiometric and Nonstoichiometric Ultrathin Fe_3O_4(111) Films on Al_2O_3(0001). *J. Appl. Phys.* **2004**, *96*, 1165−1169.
(82) de Groot, F. M. F.; Fuggle, J. C.; Thole, B. T.; Sawatzky, G. A. 2*p* X-ray Absorption of 3*d* Transition-Metal Compounds: An Atomic Multiplet Description Including the Crystal Field. *Phys. Rev. B* **1990**, *42*, 5459−5468.
(83) Thole, B. T.; Carra, P.; Sette, F.; van der Laan, G. X-ray Circular Dichroism as a Probe of Orbital Magnetization. *Phys. Rev. Lett.* **1992**, *68*, 1943−1946.
(84) Carra, P.; Thole, B. T.; Altarelli, M.; Wang, X. X-ray Circular Dichroism and Local Magnetic Fields. *Phys. Rev. Lett.* **1993**, *70*, 694−697.
(85) Lee, K.; Kim, D. H.; Hwang, J.; Lee, K.; Yoon, S.; Suh, B. J.; Kim, K. H.; Kim, J.-Y. K.; Jang, Z. H.; Kim, B.; et al. Size-Dependent Structural Evolution of the Biomineralized Iron-Core Nanoparticles in Ferritins. *Appl. Phys. Lett.* **2013**, *102*, 133703/1−4.
(86) Guyodo, Y.; Sainctavit, P.; Arrio, M.-A.; Carvallo, C.; Lee Penn, R.; Erbs, J. J.; Forsberg, B. S.; Morin, G.; Maillot, F.; Lagroix, F.; et al. X-ray Magnetic Circular Dichroism Provides Strong Evidence for Tetrahedral Iron in Ferrihydrite. *Geochem. Geophys. Geosyst.* **2012**, *13*, Q06Z44/1−9.
(87) Coker, V. S.; Pearce, C. I.; Lang, C.; van der Laan, G.; Pattrick, R. A.; Telling, N. D.; Schüler, D.; Arenholz, E.; Lloyd, J. R. Cation Site Occupancy of Biogenic Magnetite Compared to Polygenic Ferrite Spinels Determined by X-ray Magnetic Circular Dichroism. *Eur. J. Mineral.* **2007**, *19*, 707−716.
(88) Pearce, C. I.; Henderson, C. M. B.; Pattrick, R. A. D.; van der Laan, G.; Vaughan, D. J. Direct Determination of Cation Site Occupancies in Natural Ferrite Spinels by $L_{2,3}$ X-ray Absorption Spectroscopy and X-ray Magnetic Circular Dichroism. *Am. Mineral.* **2006**, *91*, 880−893.
(89) Thole, B. T.; van der Laan, G. Branching Ratio in X-ray Absorption Spectroscopy. *Phys. Rev. B* **1988**, *38*, 3158−3171.
(90) Tromp, M.; Moulin, J.; Reid, G.; Evans, J. Cr K-Edge XANES Spectroscopy: Ligand and Oxidation State Dependence: What is Oxidation State? *AIP Conf. Proc.* **2007**, *882*, 669−701.
(91) Farges, F. Chromium Speciation in Oxide-type Compounds: Application to Minerals, Gems, Aqueous Solutions and Silicate Glasses. *Phys. Chem. Miner.* **2009**, *36*, 463−481.
(92) Glatzel, P.; Smolentsev, G.; Bunker, G. The Electronic Structure in 3d Transition Metal Complexes: Can We Measure Oxidation States? *J. Phys.: Confer. Ser.* **2009**, *190*, 012046/1−11.
(93) Bunker, G., Ed. In *Introduction to XAFS: A Practical Guide to X-ray Absorption Fine Structure Spectroscopy*; Cambridge University Press: U.K., 2010.
(94) de Vries, A. H.; Hozoi, L.; Broer, R. Origin of the Chemical Shift in X-Ray Absorption Near-Edge Spectroscopy at the Mn K-Edge in Manganese Oxide Compounds. *Int. J. Quantum Chem.* **2003**, *91*, 57−61.
(95) It should be noted that we are just adding normalized XANES spectra, which corresponds to the absorption per Fe atom. Hence, the percentages used in the weighted sums refer to the XANES spectra and not to the Fe molar weight of each compound, which are indicated by the quantities in parentheses.
(96) Jeyadevan, B.; Shinoda, K.; Justin, R. J.; Matsumoto, T.; Sato, K.; Takahashi, H.; Sato, Y.; Tohji, K. Polyol Process for Fe-based Hard(fct-FePt) and Soft(FeCo) Magnetic Nanoparticles. *IEEE Trans. Magn.* **2005**, *42*, 3030−3035.

(97) The Fe^{2+}/Fe^{3+} ratio and vacancies distribution are a priori unknown. By this reason we have performed the calculations by modifying the cell parameter of both magnetite and maghemite to take into account the different structural environment associated to both Fe^{2+} and Fe^{3+} ions in the spinel structure.

(98) García, J.; Subías, G.; Herrero-Martn, J.; Blasco, J.; Cuartero, V.; Sánchez, M. C.; Mazzoli, C.; Yakhou, F. Reexamination of the Temperature Dependences of Resonant Reflections in Highly Stoichiometric Magnetite. *Phys. Rev. Lett.* **2009**, *102*, 176405/1−4.